

Update: Progress toward fusion energy breakeven and gain as measured against the Lawson criteria

Update: Progress toward fusion energy breakeven and gain as measured against the Lawson criteria

S. E. Wurzel¹ and S. C. Hsu²

¹⁾Fusion Energy Base

²⁾Lowercarbon Capital

(*Electronic mail: sam@fusionenergybase.com)

(Dated: 11 June 2025)

This paper is an update to our earlier paper “Progress toward fusion energy breakeven and gain as measured against the Lawson criterion” [Phys. Plasmas **29**, 062103 (2022)]. Plots of Lawson parameter and triple product vs. ion temperature and triple product vs. date achieved are updated with recently published experimental results. A new plot of scientific energy gain vs. date achieved is included. Additionally, notes on new experimental results, clarifications, and a correction are included.

I. INTRODUCTION

This paper is an update to our earlier paper “Progress toward fusion energy breakeven and gain as measured against the Lawson criterion,”¹ which we refer to hereafter as the “original paper.” Since its publication in 2022, both fusion researchers and investors have encouraged us to provide updated plots and data tables highlighting the continued physics progress of fusion experiments.

The purpose of this paper is therefore to update the set of experimentally achieved physics results with data published in peer-reviewed publications since the beginning of 2022. These include results from the C-2W experiment (TAE Technologies), the Fusion Z-pinch Experiment (FuZE) (Zap Energy), the Joint European Torus (JET) (UK Atomic Energy Authority), the Magnetized Liner Inertial Fusion (MagLIF) experiment (Sandia National Laboratories), the National Ignition Facility (NIF) (Lawrence Livermore National Laboratory), the OMEGA laser facility (University of Rochester’s Laboratory for Laser Energetics), the Plasma Compression System (PCS) and Plasma Injector 3 (PI3) experiments (General Fusion), and the ST40 spherical tokamak (Tokamak Energy). Also included is a clarification of nomenclature, a slight reframing of the ICF (inertial confinement fusion) ignition condition, a discussion of the triple product as a metric, a correction, and a new plot of scientific energy gain Q_{sci} vs. date achieved.

This paper is organized as follows. Section II provides updated and new plots, including descriptions of changes from the original paper. Section III provides clarifications and a correction to the original paper. Section IV discusses the new experimental results included in this paper. Section V provides updated and new data tables.

II. PLOTS

This section provides updated plots of compiled Lawson parameters vs. ion temperatures T_i (Fig. 1), compiled triple products vs. T_i (Fig. 2), record triple products vs. date achieved (Fig. 3), and a new plot of Q_{sci} vs. date achieved (Fig. 4). These plots are generated from an updated code,

which is available for download.² There are seven changes from the plots in the original paper:

1. Additional data points from C-2W, FuZE, JET, MagLIF, NIF, OMEGA, PCS, PI3, and ST-40 are included.
2. The contour colors corresponding to different values of $Q_{\text{sci}}^{\text{MCF}}$ in Figs. 1 and 2, as well as the corresponding lines in Fig. 3, are no longer arbitrary. Instead, these contours are displayed in red, based on an advanced-tokamak (AT) model with associated temperature and density profiles and a range of impurity levels, which are described in Sec. IV of the original paper. The positions of the contours are unchanged. Different transparency levels are used to indicate different values of $Q_{\text{sci}}^{\text{MCF}}$. This change is intended to emphasize that the contours shown are specific to the AT, although they are generally representative of magnetic confinement fusion (MCF) and are therefore labeled as $Q_{\text{sci}}^{\text{MCF}}$.
3. The black ignition curves in Figs. 1 and 2, the ignition lines in Fig. 3, and data points for NIF and OMEGA (where stagnation time τ_{stag} was reported) have all been increased along the y-axis by a factor of three. This is because the previous adjustment factor of 1/3 to τ_{stag} of an ICF hot spot to obtain the idealized confinement time τ (discussed in Sec. IV.B.2 of the original paper) is now reflected as a factor-of-three increase along the y-axis of the ignition curve. This adjustment is discussed further in Sec. III C.
4. The data points representing NIF shot N210808 in Figs. 1, 2, and 3 include a surrounding gold box to indicate that the shot achieved hot-spot ignition and the onset of propagating burn and is therefore the terminal data point for NIF on those figures. Additionally, a dashed black-and-gold line appears in Fig. 3 indicating the lower required triple product to achieve hot-spot ignition and the onset of propagating burn at $T_i = 10$ keV, which N210808 (but not earlier NIF shots) exceeded. These changes are discussed further in Sec. III D.
5. The anticipated timelines for SPARC and ITER have been updated based on recent announcements.^{3,4}

6. Where known, Figs. 3 and 4 utilize the exact date on which the experiment occurred (only the year was used in the original paper). We welcome readers to send us the full date for any experiments showing only the year in Tables I–IV.
7. In all figures, we have separated the experimental category of "Laser ICF" into "Laser Indirect Drive" and "Laser Direct Drive" to track the progress of each independently.

In addition to the above changes, we introduce a new plot (Fig. 4) of Q_{sci} vs. date achieved. For this plot, we recognize only actual fusion energy released (for ICF) or fusion power (for MCF, see the plot caption for details). The inclusion of this new graph is a recognition of scientific energy breakeven ($Q_{\text{sci}} > 1$) having been achieved for the first time in a controlled-fusion experiment⁵ shortly after the publication of our original paper. The most relevant figure of merit for such high-performing experiments is simply Q_{sci} . With even higher performance, a useful metric could be wall-plug gain Q_{wp} as defined in Eq. (27) of the original paper.

III. CLARIFICATIONS AND CORRECTIONS

A. The term "Lawson criterion"

In the original paper (Sec. I, first paragraph), we stated:

"The required temperature and Lawson parameter for self-heating from charged fusion products to exceed all losses is known as the *Lawson criterion*. A fusion plasma that has reached these conditions is said to have achieved *ignition*."

It would have been clearer to have used *Lawson criteria for ignition* instead of *Lawson criterion* because there are two separate requirements (product of density n and energy confinement time τ_E or pulse duration τ , and, separately, T_i), so the plural "criteria" is appropriate. Furthermore, although "Lawson criteria" (or "Lawson criterion") is usually assumed to mean the requirements for ignition, Lawson originally described "criteria for a useful thermonuclear reactor,"⁶ which he determined to be an energy gain of 2. Therefore, when referring to the *Lawson criteria*, it is worthwhile to specify the criteria being discussed, e.g., the criteria for ignition or the criteria for a specific value of energy gain.

B. Necessity of ignition

In the original paper (Sec. I, first paragraph), we stated:

"Although ignition is not required for a commercial fusion-energy system, ..."

It would have been more accurate to state "Although ignition is not required for a commercial fusion-energy system for certain fusion approaches, ..." While MCF and MIF concepts

may not strictly need to reach ignition for a commercially viable system, ICF concepts likely need to achieve ignition to realize the energy gains needed for a commercially viable system.

C. Reframing the ICF ignition condition using experimentally measured τ_{stag}

In Sec. IV.B.2 of the original paper, we described reducing experimentally measured values of τ_{stag} , which is defined as the full width at half maximum (FWHM) of the burn duration, by a factor of three. This adjustment was based on the requirement for ICF hot-spot ignition and the onset of propagating burn (herein referred to as simply "ignition" for both direct- and indirect-drive) as described by Christopherson et al.⁷

In this update, instead of reducing the measured τ_{stag} by a factor of three, we increase the ignition threshold of the Lawson parameter (and triple product) from the idealized case by the same factor of three. As a result, all ICF data points with reported τ_{stag} (except FIREX) and the ignition contour itself are shifted upward along the y-axis by a factor of three.

The revised ignition contour is now labeled $(n\tau_{\text{stag}})_{\text{ig,hs}}^{\text{ICF}}$ to emphasize that the criterion is based on the experimentally measurable stagnation time, τ_{stag} , rather than the idealized stagnation duration τ . This updated formulation aligns conceptually with our approach to MCF, where Q_{sci} contours are adjusted to account for deviations from the idealized case (i.e., flat profiles and no impurities). The physical ICF ignition condition can be derived from the "Christopherson criterion" $f_\alpha \geq 1.4$, where

$$f_\alpha = \frac{1}{2} \frac{\theta_\alpha E_\alpha}{E_{\text{hs}}}. \quad (1)$$

Here, θ_α is the fraction of alpha-particle energy deposited in the hot spot, E_α the total alpha energy from fusion reactions, and E_{hs} the internal energy of the hot spot at bang time (time of maximum neutron production). Physically, f_α is the ratio of alpha-particle energy deposited into the hot spot to hot-spot internal energy at bang time. Because approximately half of the alphas have deposited their energy by bang time, a factor of 1/2 is included.

In Sec. III.F of the original paper, the idealized ignition condition was derived by balancing the total alpha-particle energy with the internal energy of an idealized hot spot (which assumes an instantaneous temperature rise sustained over a duration τ). Applying the physical ignition condition above leads to the ignition threshold in terms of τ_{stag} :

$$(n\tau_{\text{stag}})_{\text{ig,hs}}^{\text{ICF}} = \frac{2f_\alpha}{\theta_\alpha} \frac{12T}{\langle \sigma v \rangle \epsilon_\alpha}. \quad (2)$$

Substituting $f_\alpha = 1.4$ and $\theta_\alpha = 0.93$ (for NIF conditions⁷) results in a threefold increase in the ignition threshold relative to the idealized case. Although this is intended to be a requirement for both direct- and indirect-drive hot-spot ignition and onset of propagating burn, the factor-of-three increase from the ideal case would vary if θ_α in Eq. 2 differs from 0.93.

D. Limitations of the triple product as a metric

The triple product is a convenient figure of merit for evaluating progress *toward* fusion breakeven and gain because it is a single scalar value that can be compared across experiments and tracked over time, as in Fig. 3. Mathematically, it is the area of a rectangle defined by the origin and any point within the domain of Fig. 1 (assuming linear rather than logarithmic axes). The minimum triple product for a particular contour of Q_{sci} would correspond to the minimum-area rectangle with a vertex on the contour.

As emphasized in the original paper, the triple product does *not* uniquely map to a value of Q_{sci} (in the case of MCF) or to the threshold of hot-spot ignition and onset of propagating burn (in the case of ICF). However, specific combinations of T_i and $n\tau_E^*$ (in the case of MCF) or $n\tau_{\text{stag}}$ (in the case of ICF) do map to a unique value of Q_{sci} or the ignition threshold, respectively. For this reason, Fig. 3 indicates the assumed T_i for the various horizontal lines. In general, only density and (energy) confinement time may be traded off with each other without altering the achieved gain. *Temperature cannot be traded off with the other two quantities and should be carefully scrutinized when evaluating any triple-product claim.*

In the context of ICF, further improvements in energy gain beyond ignition are driven by details such as the degree of propagating burn and burn-up fraction of the surrounding fuel layer that are not directly encapsulated by the triple product. Therefore, beyond ignition, the triple product is no longer a useful metric to quantify improvements in ICF performance. In fact, the triple product for the highest-performing NIF shots (based on Q_{sci}) declines due to propagating burn, which causes more rapid disassembly and therefore lower values of τ_{stag} . For these reasons, shot N210808 is the terminal data point for NIF in Figs. 1, 2, and 3.

In the context of MCF, improvements in triple product beyond scientific energy breakeven should correlate with increased energy gain if the temperature is in the range for which this occurs (approximately 10–30 keV for deuterium-tritium; see Fig. 2). A limitation of the triple product as a figure of merit in the MCF context is illustrated in Fig. 3, where TFTR holds the triple-product record for tokamaks due to its exceptionally high ion temperatures (> 40 keV) achieved in 1996. In contrast, JET achieved the highest Q_{sci} in a tokamak in 1997 (see Fig. 4). However, this shot was not a triple-product record for tokamaks and therefore does not appear in Fig. 3.

E. Correction

Equation (23) of the the original paper had “ $\langle\sigma v\rangle(T)$ ” in the denominator, which was intended to indicate that $\langle\sigma v\rangle$ is a function of T . Because this introduces ambiguity and because the rest of the original paper does not explicitly show the T dependence of $\langle\sigma v\rangle$, Eq. (23) of the original paper should be

corrected:

$$nT\tau_E = \frac{3T^2}{(f_c + Q_{\text{fuel}}^{-1})\langle\sigma v\rangle\varepsilon_F/4 - C_B T^{1/2}}. \quad (3)$$

IV. NEW DATA

Since the original paper was published in 2022, new experimental results have been published. Notes on each new data point are included in this section.

A. NIF

On August 8th, 2021 the National Ignition Facility (NIF) achieved hot-spot ignition and the onset of propagating burn, but not ignition according to the definition⁸ of the National Academies of Sciences, Engineering, and Medicine (NASEM), the details of which are discussed below. When we submitted our original paper for publication in December 2021, the only publication describing this experimental shot (N210808) was an initial technical report,⁹ from which we extracted relevant parameters. Since then, peer-reviewed publications^{5,10} have described this shot in detail and included minor adjustments to the reported measurements; the adjustments are used in this paper.

On December 5th, 2022, ignition according to the NASEM definition was achieved in shot N221204. NASEM defined ignition as the “ratio of fusion yield to laser energy” exceeding unity,⁸ which corresponds to our definition of scientific energy breakeven. Shot N221204 crossed this threshold, achieving $Q_{\text{sci}} = 1.5$. In May 2024, LLNL announced¹¹ that four additional shots achieved ignition, reaching values up to $Q_{\text{sci}} \approx 2.4$. In May 2025, LLNL announced¹² that $Q_{\text{sci}} = 4.13$ was achieved in the prior month, with eight total shots having achieved $Q_{\text{sci}} > 1$. As of this writing, details of the seven additional shots have not yet been published in a peer-reviewed journal, but they are included in Fig. 4 and Table IV.

We also include minor updates to the reported, measured parameters achieved in shots N210207, N210307, N210808, as well as newer shots N220919 and N221204, based on the most recent peer-reviewed publication providing these data.⁵

Based on the discussion of Sec. IIID, N210808 is the final NIF result included in Table III and in Figs. 1, 2, and 3, with subsequent results included in Table IV and Fig. 4.

B. OMEGA

Details of OMEGA’s 2021 experimental campaign were published¹³ in early 2024 showing improved performance and the first achievement of fuel energy gain (ratio of fusion energy to the hot-spot internal energy greater than unity) in a direct-drive laser-ICF experiment. This result is the highest achieved Q_{sci} in a direct-drive laser-ICF experiment that has been published, having achieved $Q_{\text{sci}} = 0.02$, and is included in Table IV and Fig. 4.

C. MagLIF

A new publication¹⁴ reports record results for MagLIF. Shot z3289 achieved a high triple product, exceeding $10^{21} \text{ keV m}^{-3} \text{ s}$. Note that although it appears at the red $Q_{\text{sci}}^{\text{MCF}} = 1$ line in Fig. 3, it does not correspond to that line because T_i was too low (2.6 keV), and the red lines assume a temperature of approximately 20 keV (and advanced-tokamak profiles). Fig. 1 more clearly shows the relative performance of the MagLIF results and the benefit that higher temperature would have in advancing MagLIF performance. Because MagLIF experiments utilize pure deuterium fuel, their results are not included in Table IV nor in Fig. 4.

D. JET

Since publication of the original paper, JET has published the results of two recent deuterium-tritium experiment (DTE) campaigns, DTE2 and DTE3, which occurred in 2021 and 2023, respectively. The goals of these campaigns included demonstrating long-pulse operation and the development of experimental scenarios for ITER. These campaigns were not designed to set scientific gain or triple-product records. They did, however, achieve record levels of fusion energy produced in a single fusion experiment, with shot 99971 producing 59 MJ of fusion energy during the DTE2 campaign and shot 104522 producing 69 MJ of fusion energy during the DTE3 campaign. The scientific energy gain achieved by these shots was 0.33 and 0.37, respectively. Published temperature, density, and energy confinement time data from shot 99972 (from DTE2) and shot 104600 (from DTE3) were extracted and are displayed in Figs. 1 and 2.

E. ST40

Tokamak Energy published results from ST40¹⁵ demonstrating a central T_i of 9.6 keV and a central ion density n_i of $5.5 \times 10^{19} \text{ m}^{-3}$ at a flat-top time of 56 ms into the pulse. To evaluate τ_E^* , we take the stored thermal energy to be 70% of 35 kJ because the publication states “fast ions account for approximately 30% of the stored energy,” and their Fig. 1 indicates a stored energy of 35 kJ at 56 ms. The absorbed heating power includes 92% of 1.6 MW of neutral-beam heating (accounting for 8% maximum reported shine-through) and 0.5 MW of ohmic heating for a total absorbed heating power of approximately 2 MW. The τ_E^* is therefore 12 ms, and the triple product is evaluated to be $6.3 \times 10^{18} \text{ keV m}^{-3} \text{ s}$, which is in agreement with that reported by Tokamak Energy.

A separate publication¹⁶ reported results for shot 104949, which, if scaled up in size, would be projected to achieve a burning plasma, but the shot did not (and was not intended to) set a record for fusion-energy yield. Due to the high achieved pressure, it set a laser direct-drive triple-product record, which is reflected in Table III and Fig. 3. The energy yield from this shot was extrapolated from the number of reported D-T

neutrons (energy from other fusion reactions are neglected) and is reflected in Table IV and Fig. 4.

F. FuZE

New experimental results from the FuZE experiment¹⁷ at Zap Energy indicate record performance of their stabilized Z-pinch. In shots at a plenum pressure of 200 psi, electron temperatures of 2.4 keV and electron densities of $4.9 \times 10^{23} \text{ m}^{-3}$ were reported. The energy confinement time is assumed to be 1 μs based on the flow-through time of the plasma along the pinch as discussed in the original paper. This assumption (that advection along the pinch is the dominant heat-loss mechanism) would benefit from further study.

G. C-2W

A new publication from TAE Technologies¹⁸ provides data demonstrating electron temperature $T_e \approx 1 \text{ keV}$ (to our knowledge, for the first time ever) in a field-reversed configuration (FRC) (shot 122588 on C-2W). Although the density of this shot was not published, the density was in the range $1.2\text{--}1.4 \times 10^{19} \text{ m}^{-3}$.¹⁹ The τ_E^* for shot 122588 is inferred to be 2 ms (from the slope of Fig. 4 of the aforementioned publication). Because T_i for previously published shots were higher ($\approx 3.5 \text{ keV}$), shot 122588 is not a triple-product record and therefore does not appear in Fig. 3.

H. PCS

A new publication²⁰ analyzes the results of General Fusion’s Plasma Compression Science (PCS) program. PCS was a campaign of magnetized-target-fusion (MTF) experiments in which a compact toroid was formed by a Marshall gun and injected into a spheroidal chamber with a current-carrying center post. The combined poloidal (due to magnetization during formation) and toroidal (due to the current-carrying center post) magnetic fields form a spherical tokamak within the chamber. At this point, a high-explosive charge is detonated to implode the chamber (acting like a liner) and compress the plasma.

Key parameters for this concept (and all fusion concepts that involve compressional heating) are the particle confinement time τ_p , τ_E , and the time taken to compress the plasma τ_C . For density to increase during compression, $\tau_C \ll \tau_p$ is required. For the temperature to increase, the compression must occur quasi-adiabatically, i.e., $\tau_C \ll \tau_E$ is required.

In the best-performing experiment, PCS-16, τ_p was much larger than $\tau_C = 139 \mu\text{s}$, and the electron density n_e increased from $1.2 \times 10^{20} \text{ m}^{-3}$ before compression to $2.3 \times 10^{22} \text{ m}^{-3}$ at peak compression. However, because $\tau_{E_e} \approx 50 \mu\text{s}$ was less than half of $\tau_C = 139 \mu\text{s}$, the pre-compression T_e of 200 eV did not increase, and the peak T_i only reached 629 eV from a pre-compression value of 600 eV.

The liner begins to move at $t = 300 \mu\text{s}$, at which point the plasma is uncompressed. At this time n_e is $1.25 \times 10^{20} \text{ m}^{-3}$, T_e is 207 eV, and T_i is 600 eV. The pre-compression τ_E is reported as $84 \mu\text{s}$ based on MHD simulations that matched experimental data on the decay of measured magnetic fields. The pre-compression triple product is therefore $6.3 \times 10^{15} \text{ keV m}^{-3} \text{ s}$.

At $t = 405 \mu\text{s}$, the compressed plasma begins to lose MHD stability. We evaluate the parameters at this point of the compression sequence when the average n_e is $5 \times 10^{20} \text{ m}^{-3}$, the T_e is approximately 180 eV, and the T_i is 627 eV. The energy confinement time of ions at this point τ_{Ei} is reported as $122 \mu\text{s}$. We use this value as the effective τ_E because it encapsulates all cooling channels for ions and is shorter than the electron-ion equilibration time τ_{eq} of $693 \mu\text{s}$. This implies that the dominant cooling mechanism of ions in this particular case is not heat transfer to electrons.

We caution that the effective confinement time τ_{eff}^1 could be reduced from τ_E by half if τ_{stag} (also not reported) is of the same order as τ_E at peak compression. In this case, the effective triple product would be reduced by the same factor.

I. PI3

General Fusion recently published results²¹ for the upgraded PI3 spherical tokamak, which began operation in 2021. Although intended to study spherical tokamaks to understand the timescales needed for compression in future machines, PI3 experiments do not perform compression. Shot 21 100 reported a T_i of 400 eV, a central n_e of $4 \times 10^{19} \text{ m}^{-3}$, and a τ_E of approximately 12 ms.

V. TABLES

Tables I–III, which provide the data for Figs. 1–3, are updated from their corresponding tables in the original paper and include new data points and new references upon which the new data points are based. Data on stellarators has been shifted from Table I to Table II to keep each table to a single page. Table IV provides the numerical data for Fig. 4. For all tables, data unchanged from the original paper cite the original paper (which cites the primary source). Updated or new data cite the primary source.

ACKNOWLEDGMENTS

We acknowledge Julia Haack and Luigi Di Pace for alerting us to the ambiguity in Eq. (23) of the original paper. Thanks to Mikhail Maslov for providing the dates of specific JET shots, Rich Hawryluk for providing the dates of TFTR shots and feedback on nomenclature, Myles Hildebrand for providing further details on PCS and PI3, Hiroshi Gota for providing further details on recent C-2W shots, and both Leland Ellison and Alison Christopherson for discussions about the adjust-

ment of the confinement time and the requirements for ignition in ICF experiments.

DATA AVAILABILITY STATEMENT

Data sharing is not applicable to this paper as no new data were created or analyzed in this study. The extracted data from other publications and codes used to make the plots and tables in this paper are available for download.²

¹S. E. Wurzel and S. C. Hsu, Phys. Plasmas **29**, 062103 (2022).

²<https://github.com/swurzel/lawson-criterion-paper>.

³Commonwealth Fusion Systems, “SPARC: Fusion energy demonstration,” (2024), accessed: 2024-12-06. Available at <https://cfs.energy/technology/sparc>.

⁴ITER Organization, “New Baseline to Prioritize Robust Start to Exploitation,” (2024), accessed: 2024-08-23. Available at <https://www.iter.org/newsline/-/4056>.

⁵H. Abu-Shwareb, R. Acree, P. Adams, J. Adams, B. Addis, R. Aden, P. Adrian, B. B. Afeyan, M. Aggleton, and et. al., Phys. Rev. Lett. **132** (2024), 10.1103/physrevlett.132.065102.

⁶J. D. Lawson, “Some Criteria for a Useful Thermonuclear Reactor,” Tech. Rep. GP/R 1807 (Atomic Energy Research Establishment, 1955) https://www.euro-fusion.org/fileadmin/user_upload/Archive/wp-content/uploads/2012/10/dec05-aere-gpr1807.pdf.

⁷A. R. Christopherson, R. Betti, and J. D. Lindl, Phys. Rev. E **99** (2019).

⁸National Research Council, *Review of the Department of Energy’s Inertial Confinement Fusion Program* (National Academies Press, Washington, DC, 1997).

⁹O. A. Hurricane et. al., “Lawson criterion for ignition exceeded in an inertial fusion experiment,” Technical Report No. LLNL-JRNL-830617 (2022).

¹⁰A. L. Kratcher, A. B. Zylstra, D. A. Callahan, O. A. Hurricane, C. R. Weber, D. S. Clark, C. V. Young, J. E. Ralph, D. T. Casey, A. Pak, O. L. Landen, B. Bachmann, K. L. Baker, L. Berzak Hopkins, S. D. Bhandarkar, J. Biner, R. M. Bionta, N. W. Birge, T. Braun, T. M. Briggs, P. M. Celliers, H. Chen, C. Choate, L. Divol, T. Döppner, D. Fittinghoff, M. J. Edwards, M. Gatou Johnson, N. Gharibyan, S. Haan, K. D. Hahn, E. Hartouni, D. E. Hinkel, D. D. Ho, M. Hohenberger, J. P. Holder, H. Huang, N. Izumi, J. Jeet, O. Jones, S. M. Kerr, S. F. Khan, H. Geppert Kleinrath, V. Geppert Kleinrath, C. Kong, K. M. Lamb, S. Le Pape, N. C. Lemos, J. D. Lindl, B. J. MacGowan, A. J. Mackinnon, A. G. MacPhee, E. V. Marley, K. Meaney, M. Millot, A. S. Moore, K. Newman, J.-M. G. Di Nicola, A. Nikroo, R. Nora, P. K. Patel, N. G. Rice, M. S. Rubery, J. Sater, D. J. Schlossberg, S. M. Sepke, K. Sequoia, S. J. Shin, M. Stadermann, S. Stoupin, D. J. Strozzi, C. A. Thomas, R. Tommasini, C. Trosseille, E. R. Tubman, P. L. Volegov, C. Wild, D. T. Woods, and S. T. Yang, Phys. Rev. E **106**, 025201 (2022).

¹¹C. Osolin, The Bridge, The Magazine of IEEE-Eta Kappa Nu **120**, 11 (2024), available at https://magazines.ieee.org/hkn/library/page/issue_2_2024/12/.

¹²T. Lynch, LLNL Inertial Fusion Energy Website (2025), available at <https://ife.llnl.gov/llnl-experts-foster-national-fusion-energy-ecosystem-ife-star-confe>

¹³C. A. Williams, R. Betti, V. Gopalaswamy, J. P. Knauer, C. J. Forrest, A. Lees, R. Ejaz, P. S. Farmakis, D. Cao, P. B. Radha, K. S. Anderson, S. P. Regan, V. Y. Glebov, R. C. Shah, C. Stoeckl, S. Ivancic, K. Churnetski, R. T. Janezic, C. Fella, M. J. Rosenberg, M. J. Bonino, D. R. Harding, W. T. Shmyda, J. Carroll-Nellenback, S. X. Hu, R. Epstein, T. J. B. Collins, C. A. Thomas, I. V. Igumenshchev, V. N. Goncharov, W. Theobald, K. M. Woo, J. A. Marozas, K. A. Bauer, S. Sampat, L. J. Waxer, D. Turnbull, P. V. Heuer, H. McClow, L. Ceurvorst, W. Scullin, D. H. Edgell, M. Koch, D. Bredesen, M. G. Johnson, J. A. Frenje, R. D. Petrasso, C. Shulberg, M. Farrell, J. Murray, D. Guzman, B. Serrato, S. F. B. Morse, M. Labuzeta, C. Deeney, and E. M. Campbell, Nature Phys. **20**, 758 (2024).

¹⁴P. F. Knapp, M. E. Glinsky, M. A. Schaeuble, C. A. Jennings, M. Evans, J. Gunning, T. J. Awe, G. A. Chandler, M. Geissel, M. R. Gomez, K. D. Hahn, S. B. Hansen, E. C. Harding, A. J. Harvey-Thompson, S. Humane,

TABLE I. Data for tokamaks and spherical tokamaks.

Project	Concept	Date	Shot identifier	Reference	T_{e0} (keV)	n_{e0} (m $^{-3}$)	τ_E^* (s)	$n_{e0}\tau_E^*$ (m $^{-3}$ s)	$n_{e0}T_{e0}\tau_E^*$ (keV m $^{-3}$ s)
T-3	Tokamak	1969	$H_z = 25\text{ kOe}, I_z = 85\text{ kA}$ discharges	1	0.3	2.25×10^{19} [‡]	2.25×10^{19}	0.003	6.8×10^{16}
ST	Tokamak	1971	10cm limiter, 42 kA	1	0.5	4×10^{19} [‡]	4×10^{19}	0.0034	1.4×10^{17}
ST	Tokamak	1972	12cm limiter	1	0.4	0.8	6×10^{19} [‡]	0.01	6.0×10^{17}
TFR	Tokamak	1974	Molybdenum limiter	1	0.95	1.8	7.1×10^{19} [‡]	0.019	1.3×10^{18}
PLT	Tokamak	1976	22149-231	1	1.54	1.86×10^{19} [‡]	5.2×10^{19}	0.04	2.1×10^{18}
Alcator A	Tokamak	1978	8.7T discharge	1	0.8	0.9	1.5×10^{21} [‡]	1.5×10^{21}	0.02
TFR	Tokamak	1981	Iconel limiter	1	0.95	1.2	1.61×10^{20} [‡]	1.61×10^{20}	0.034
TFR	Tokamak	1982	Carbon limiter	1	0.95	1.5	9×10^{19} [‡]	9×10^{19}	0.025
Alcator C	Tokamak	1984	Multiple pellet injection	1	1.5	1.5×10^{21} [‡]	1.5×10^{21}	0.052	7.8×10^{19}
ASDEX	Tokamak	1988	23349-57	1	0.8	1	7.50×10^{19} ^{‡*}	—	0.12
JET	Tokamak	1991-11-02	26087	1	18.6	10.5	4.1×10^{19}	5.1×10^{19}	$0.8^{\#}$
JET	Tokamak	1991-11-04	26095	1	22.0	11.9	3.4×10^{19}	4.5×10^{19}	$0.8^{\#}$
JET	Tokamak	1991-11-09	26148	1	18.8	9.9	2.4×10^{19}	3.6×10^{19}	$0.6^{\#}$
TFTR	Tokamak	1992-10-29	68522	1	29.0	11.7	6.8×10^{19}	9.6×10^{19}	$0.18^{\#}$
JT-60U	Tokamak	1994	17110	1	37	12	4.2×10^{19}	5.5×10^{19}	$0.3^{\#}$
TFTR	Tokamak	1994-05-27	76778	1	44	11.5	6.3×10^{19}	8.5×10^{19}	$0.19^{\#}$
TFTR	Tokamak	1994-11-02	80539	1	36	13	6.7×10^{19}	1.02×10^{20}	$0.17^{\#}$
TFTR	Tokamak	1995-02-17	83546	1	43	12.0	6.6×10^{19}	8.5×10^{19}	$0.28^{\#}$
JT-60U	Tokamak	1996	E26939	1	45.0	10.6	4.35×10^{19}	6×10^{19}	$0.26^{\#}$
JT-60U	Tokamak	1996	E26949	1	35.5	11.0	4.3×10^{19}	5.85×10^{19}	$0.28^{\#}$
DIII-D	Tokamak	1997	87977	1	18.1	7.5	8.5×10^{19}	1×10^{20}	$0.24^{\#}$
JET	Tokamak	1997-10-31	42976	1	28	14	3.3×10^{19}	4.1×10^{19}	$0.51^{\#}$
START	Spherical Tokamak	1998	35533	1	0.2 [†]	0.2	1.02×10^{20} ^{‡*}	—	0.003
JT-60U	Tokamak	1998	E31872	1	16.8	7.2	4.8×10^{19}	8.5×10^{19}	$0.69^{\#}$
MAST	Spherical Tokamak	2006	14626	1	3	2	3×10^{19} [‡]	3×10^{19}	0.05
NSTX	Spherical Tokamak	2009	129041	1	1.2	1.2	5×10^{19} [‡]	5×10^{19}	0.08
EAST	Tokamak	2012	41195	1	0.9	—	3×10^{19} [‡]	3×10^{19}	0.04
EAST	Tokamak	2012	41079	1	1.2 [†]	1.2	2×10^{19} [‡]	2×10^{19}	0.04
EAST	Tokamak	2014	48068	1	1.2	—	6.1×10^{19} [‡]	6.1×10^{19}	0.037
KSTAR	Tokamak	2014	7081	1	2	—	4.80×10^{19} ^{‡*}	—	0.1
EAST	Tokamak	2015	56933	1	2.1	1.8	8.5×10^{19} [‡]	8.5×10^{19}	0.054
C-Mod	Tokamak	2016	1160930042	1	6 [†]	6	2×10^{20} [‡]	2×10^{20}	0.054
EAST	Tokamak	2016	71320	1	1.8	2.0	5.5×10^{19} [‡]	5.5×10^{19}	0.036
C-Mod	Tokamak	2016	1160930033	1	2.5 [†]	2.5	5.5×10^{20} [‡]	5.5×10^{20}	0.054
ASDEX-U	Tokamak	2016	32305	1	8	5	5×10^{19} [‡]	5×10^{19}	0.056
EAST	Tokamak	2018	78723	1	1.94	—	5.58×10^{19} [‡]	5.58×10^{19}	0.045
Globus-M2	Spherical Tokamak	2019	37873	1	1.2	—	1.19×10^{20} ^{‡*}	—	0.01
P13	Spherical Tokamak	2021	21100	21	0.4	0.350	4×10^{19} [‡]	4×10^{19}	0.012
JET	Tokamak	2021-12-21	99972	22	11	—	8.5×10^{19} [‡]	8.5×10^{19}	0.23
ST40	Spherical Tokamak	2022	10009	15	9.6	3	5.5×10^{19}	9×10^{19}	0.012
JET	Tokamak	2023-10-09	104600	23 and 24	7 [†]	7	9×10^{19} [‡]	9×10^{19}	0.23
SPARC	Tokamak	2027	Projected	1	20	22	4×10^{20} [‡]	4×10^{20}	0.77
ITER	Tokamak	2039	Projected	25-29	20	—	1×10^{20} [‡]	1×10^{20}	3.7

^{*} Peak value of density or temperature has been inferred from volume-averaged value as described in Sec. IV A 4 of the original paper.¹[†] Ion temperature has been inferred from electron temperature as described in Sec. IV A 5 of the original paper.¹[‡] Ion density has been inferred from electron density as described in Sec. IV A 5 of the original paper.¹# Energy confinement time τ_E (JET/JT-60) method as described in Sec. IV A 6 of the original paper.¹

TABLE II. Data for other MCF (i.e. not tokamaks or spherical tokamaks) and lower-density MIF concepts.

Project	Concept	Date	Shot identifier	Reference	T_{i0} (keV)	T_{e0} (keV)	n_{i0} (m $^{-3}$)	n_{e0} (m $^{-3}$)	τ_E^* (s)	$n_{i0} T_{i0} \tau_E^*$ (m $^{-3}$ s)	$n_{e0} T_{e0} \tau_E^*$ (keV m $^{-3}$ s)
ZETA	Pinch	1957	140 kA - 180kA discharges	1	0.09	$1 \times 10^{20\ddagger}$	1×10^{20}	0.0001	1.0×10^{16}	9.0×10^{14}	
Model C	Stellarator	1969	ICRH heated	1	0.2^\dagger	0.2	$5 \times 10^{18\ddagger}$	5×10^{18}	5.0×10^{14}	1.0×10^{14}	
ETA-BETA I	RFP	1977	Summary	1	0.01	-	1×10^{21}	-	1.0×10^{15}	1.0×10^{14}	
W7-A	Stellarator	1980	Zero current	1	0.545	0.316	$9.6 \times 10^{19\ddagger}$	9.6×10^{19}	1.6×10^{18}	8.6×10^{17}	
ETA-BETA II	RFP	1984	59611	1	0.09 [†]	0.09	$3.5 \times 10^{20\ddagger}$	3.5×10^{20}	3.5×10^{16}	3.2×10^{15}	
TMX-U	Mirror	1984-02-02	2/284 S21	1	0.15	0.045	2×10^{18}	2×10^{18}	2.0×10^{15}	3.0×10^{14}	
ZT-40M	RFP	1987	320 kA discharge	1	0.33 [†]	0.33	$9.60 \times 10^{19\ddagger,*}$	-	0.0007	6.7×10^{16}	2.2×10^{16}
CTX	Spheromak	1990	Solid flux conserv	1	0.18	0.18	$4.50 \times 10^{19\ddagger,*}$	-	0.0002	9.0×10^{15}	1.6×10^{15}
LSX	FRC	1993	s ²	1	0.547	0.253	$1.30 \times 10^{21*}$	-	0.0001	1.3×10^{17}	7.1×10^{16}
MST	RFP	2001	390 kA discharge	1	0.396	0.792	$1.20 \times 10^{19\ddagger,*}$	-	0.0064 [#]	7.7×10^{16}	3.0×10^{16}
W7-AS	Stellarator	2002	H-NBI mode	1	2.28*	-	$1.10 \times 10^{20\ddagger,*}$	-	0.06	6.6×10^{18}	1.5×10^{19}
FRX-L	FRC	2003	2027	1	0.09	0.09	4×10^{22}	4×10^{22}	3.3×10^{-6}	1.3×10^{17}	1.2×10^{16}
ZaP	Z Pinch	2003	Unknown	1	0.1	-	$9 \times 10^{22\ddagger}$	9×10^{22}	3.7×10^{-7}	3.3×10^{16}	3.3×10^{15}
HSX	Stellarator	2005	QHS configuration	1	0.45 [†]	0.45	$2.5 \times 10^{18\ddagger}$	2.5×10^{18}	0.0006	1.5×10^{15}	6.8×10^{14}
FRX-L	FRC	2005	3684	1	0.18*	-	$4.81 \times 10^{22\ddagger,*}$	-	3.3×10^{-6}	1.6×10^{17}	2.9×10^{16}
TCS	FRC	2005	9018	1	0.025	0.025	$6.50 \times 10^{18\ddagger,*}$	-	4×10^{-5}	2.6×10^{14}	6.5×10^{12}
SSPX	Spheromak	2007	17524	1	0.5 [†]	0.5	$2.25 \times 10^{20\ddagger,*}$	-	0.001	2.2×10^{17}	1.1×10^{17}
GOL-3	Mirror	2007	Unknown	1	2	2	7×10^{20}	7×10^{20}	0.0009	6.3×10^{17}	1.3×10^{18}
TCSU	FRC	2008	21214	1	0.1	0.1	$1.30 \times 10^{19\ddagger,*}$	-	7.5×10^{-5}	9.7×10^{14}	9.7×10^{13}
LHD	Stellarator	2008	High triple product	1	0.47	0.47	$5 \times 10^{20\ddagger}$	5×10^{20}	0.22	1.1×10^{20}	5.2×10^{19}
RFX-mod	RFP	2008	24063	1	1 [†]	1	$3 \times 10^{19\ddagger}$	3×10^{19}	0.0025	7.5×10^{16}	7.5×10^{16}
MST	RFP	2009	w/o pellets	1	1.3	1.9	$1.2 \times 10^{19\ddagger}$	1.2×10^{19}	0.012	1.4×10^{17}	1.9×10^{17}
MST	RFP	2009	pellets	1	0.6	0.7	$4 \times 10^{19\ddagger}$	4×10^{19}	0.007	2.8×10^{17}	1.7×10^{17}
IPA	FRC	2010	Unknown	1	0.85*	-	$5.20 \times 10^{21\ddagger,*}$	-	1×10^{-5}	5.2×10^{16}	4.4×10^{16}
Yingguang-I	FRC	2015	150910-01	1	0.2*	-	$4.81 \times 10^{22\ddagger,*}$	-	1×10^{-6}	4.8×10^{16}	9.6×10^{15}
C-2U	FRC	2017	46366	1	0.68*	-	$2.47 \times 10^{19\ddagger,*}$	-	0.00024	5.9×10^{15}	4.0×10^{15}
W7-X	Stellarator	2017-12-07	W7X 20171207.006	1	3.5	3.5	$8 \times 10^{19\ddagger}$	8×10^{19}	0.22	1.8×10^{19}	6.2×10^{19}
FuZE	Z Pinch	2018	Multiple identical shots	1	1.8	-	$1.1 \times 10^{23\ddagger}$	1.1×10^{23}	1.1×10^{-6}	1.2×10^{17}	2.2×10^{17}
GDT	Mirror	2018	Multiple identical shots	1	0.45 [†]	0.45	$1.1 \times 10^{19\ddagger}$	1.1×10^{19}	0.0006	6.6×10^{15}	3.0×10^{15}
PCS	MTF	2018-06-01	PCS-16 (pre-compression)	20	0.600	0.207	$1.25 \times 10^{20\ddagger}$	1.25×10^{20}	8.4×10^{-5}	1.0×10^{16}	6.3×10^{15}
PCS	MTF	2018-06-01	PCS-16 (post-compression)	20	0.629	-	$5 \times 10^{20\ddagger}$	5×10^{20}	0.000122	6.1×10^{16}	3.8×10^{16}
C-2W	FRC	2019	107322	1	0.6*	-	$2.08 \times 10^{19\ddagger,*}$	-	0.0012	2.5×10^{16}	1.5×10^{16}
C-2W	FRC	2019	104989	1	1.0*	-	$1.30 \times 10^{19\ddagger,*}$	-	0.003	3.9×10^{16}	3.9×10^{16}
C-2W	FRC	2020	14534	1	1.8*	-	$1.30 \times 10^{19\ddagger,*}$	-	0.0015	2.0×10^{16}	3.5×10^{16}
C-2W	FRC	2021	18340	1	3.5*	-	$1.30 \times 10^{19\ddagger,*}$	-	0.005	6.5×10^{16}	2.3×10^{17}
FuZE	Z Pinch	2022	Multiple identical shots at 200psi	17	2.4 [†]	2.4	$4.9 \times 10^{23\ddagger}$	4.9×10^{23}	1×10^{-6}	4.9×10^{17}	1.2×10^{18}
C-2W	FRC	2023	122588	18 and 19	1 [†]	1	$1.69 \times 10^{19\ddagger,*}$	-	0.002	3.4×10^{16}	3.4×10^{16}

^{*} Peak value of density or temperature has been inferred from volume-averaged value as described in Sec. IV A 4 of the original paper.¹[†] Ion temperature has been inferred from electron temperature as described in Sec. IV A 5 of the original paper.¹[‡] Ion density has been inferred from electron density as described in Sec. IV A 5 of the original paper.¹# Energy confinement time τ_E (ITER/Lawson) method as described in Sec. IV A 6 of the original paper.¹

TABLE III. Data for ICF and higher-density MIIF concepts.

Project	Concept	Date	Shot identifier	Reference	$\langle T_i \rangle_n$ (keV)	T_e (keV)	$\rho R_{tot(n)}^{n/o(\alpha)}$ (g/cm 2)	YOC (Gbar)	p_{stag} (Gbar)	τ_{stag} (s)	E_{in} (J)	Y (J)	$P\tau_{stag}$ (amts)	$n\langle T \rangle_n \tau_{stag}$ (keV m $^{-3}$ s)	
NOVA	Laser Indirect Drive	1994	100 atm fill	1	0.9	—	—	16	5×10^{-11}	—	—	0.79	2.8×10^{20}	2.5×10^{20}	
OMEGA	Laser Direct Drive	2007	47210	1	2.0	—	0.182	0.1	—	—	—	1.13	1.8×10^{20}	3.6×10^{20}	
OMEGA	Laser Direct Drive	2007	47206	1	2.0	—	0.202	0.1	—	—	—	1.23	1.9×10^{20}	3.9×10^{20}	
OMEGA	Laser Direct Drive	2009	Unknown	1	1.8	—	0.240	0.1	—	—	—	1.29	2.3×10^{20}	4.1×10^{20}	
OMEGA	Laser Direct Drive	2009	55468	1	1.8	—	0.300	0.1	—	—	—	1.55	2.7×10^{20}	4.9×10^{20}	
OMEGA	Laser Direct Drive	2013	69236	1	2.8	—	—	—	18	1.15×10^{-10}	—	—	2.04	2.3×10^{20}	6.5×10^{20}
MagLIF	MagLIF	2014	22613	1	2.0	—	—	—	0.56	1.38×10^{-9}	—	—	0.76	1.2×10^{20}	2.4×10^{20}
NIF	Laser Indirect Drive	2014-03-04	N140304	1	5.5	—	—	—	222	1.63×10^{-10}	—	—	35.71	2.1×10^{21}	1.1×10^{22}
OMEGA	Laser Direct Drive	2015	77068	1	3.6	—	—	—	56	6.6×10^{-11}	—	—	3.65	3.2×10^{20}	1.2×10^{21}
MagLIF	MagLIF	2015	22850	1	2.8	—	—	—	0.6	1.62×10^{-9}	—	—	0.96	1.1×10^{20}	3.0×10^{20}
NIF	Laser Indirect Drive	2017-06-01	N170601	1	4.5	—	—	—	320	1.6×10^{-10}	1.5×10^6	4.8×10^4	50.53	3.6×10^{21}	1.6×10^{22}
NIF	Laser Indirect Drive	2017-08-27	N170827	1	4.5	—	—	—	360	1.54×10^{-10}	1.7×10^6	5.3×10^4	54.72	3.8×10^{21}	1.7×10^{22}
MagLIF	MagLIF	2018	23236	14	2.9	—	—	—	1.3	2.1×10^{-9}	—	—	2.69	2.9×10^{20}	8.5×10^{20}
MagLIF	MagLIF	2018	23179	14	3.3	—	—	—	1.2	1.8×10^{-9}	—	—	2.13	2.0×10^{20}	6.7×10^{20}
MagLIF	MagLIF	2018	23289	14	2.6	—	—	—	1.8	2×10^{-9}	—	—	3.55	4.3×10^{20}	1.1×10^{21}
FIREX	Laser Direct Drive	2019	40558	1	—	2.1	—	—	2	4×10^{-10}	—	—	0.79	1.2×10^{20}	2.5×10^{20}
NIF	Laser Indirect Drive	2019-09-18	N190918	30	4.43	—	—	—	140	1.54×10^{-10}	1.9×10^6	2.1×10^4	21.28	1.5×10^{21}	6.7×10^{21}
NIF	Laser Indirect Drive	2019-10-07	N191007	1	4.52	—	—	—	206	1.51×10^{-10}	1.9×10^6	5.3×10^4	30.70	2.1×10^{21}	9.7×10^{21}
NIF	Laser Indirect Drive	2019-11-10	N191110	30	4.54	—	—	—	169	1.66×10^{-10}	1.9×10^6	5.6×10^4	27.69	1.9×10^{21}	8.8×10^{21}
NIF	Laser Indirect Drive	2020-11-01	N201101	1	4.61	—	—	—	319	1.18×10^{-10}	—	—	37.15	2.5×10^{21}	1.2×10^{22}
NIF	Laser Indirect Drive	2020-11-22	N201122	1	4.65	—	—	—	297	1.37×10^{-10}	—	—	40.16	2.7×10^{21}	1.3×10^{22}
OMEGA	Laser Direct Drive	2021	103952	13	5.8	—	—	—	46.2	6×10^{-11}	3.0×10^4	8.7×10^2	2.74	1.5×10^{20}	8.7×10^{20}
OMEGA	Laser Direct Drive	2021	102360	13	6.0	—	—	—	34.9	6×10^{-11}	3.0×10^4	7.5×10^2	2.07	1.1×10^{20}	6.5×10^{20}
OMEGA	Laser Direct Drive	2021	102154	13	4.6	—	—	—	76.3	6×10^{-11}	3.0×10^4	6.3×10^2	4.52	3.1×10^{20}	1.4×10^{21}
NIF	Laser Indirect Drive	2021-02-07	N210207	1	5.66	—	—	—	304	1.37×10^{-10}	1.9×10^6	1.7×10^5	41.10	2.3×10^{21}	1.3×10^{22}
NIF	Laser Indirect Drive	2021-02-20	N210220	1	5.13	—	—	—	371	1.35×10^{-10}	—	—	49.43	3.0×10^{21}	1.6×10^{22}
NIF	Laser Indirect Drive	2021-03-07	N210307	5	5.55	—	—	—	323	1.38×10^{-10}	1.9×10^6	1.4×10^5	43.99	2.5×10^{21}	1.4×10^{22}
NIF	Laser Indirect Drive	2021-08-08	N210808	5	10.9	—	—	—	561	8.9×10^{-11}	1.3×10^6	49.28	1.4 $\times 10^{21}$	1.6×10^{22}	
OMEGA	Laser Direct Drive	2022	104949	16	4.6	3.8	0.160	—	78	7×10^{-11}	3.0×10^4	5.9×10^2	5.39	3.7×10^{20}	1.7×10^{21}

TABLE IV. Data for experiments which produced sufficient fusion energy to achieve appreciable values of scientific gain Q_{sci} .

Project	Concept	Date	Shot identifier	Reference	E_{in} (J)	γ (J)	P_{in} (W)	P_{F} (W)	Q_{sci}
JET	Tokamak	1991-11-09	26148	1	—	—	1.4×10^7	1.7×10^6	0.12
TFTR	Tokamak	1992-10-29	68522	1	—	—	3.1×10^7	6.5×10^4	0.00
TFTR	Tokamak	1994-05-27	76778	1	—	—	3.4×10^7	9.3×10^6	0.28
TFTR	Tokamak	1994-11-02	80539	1	—	—	4.0×10^7	1.1×10^7	0.27
TFTR	Tokamak	1995-02-17	83546	1	—	—	1.7×10^7	2.8×10^6	0.16
JET	Tokamak	1997-10-31	42976	1	—	1.4×10^7	2.6×10^7	1.6×10^7	0.63
JET	Tokamak	1997-10-31	42974	31	—	—	2.6×10^7	1.6×10^7	0.62
NIF	Laser Indirect Drive	2013-09-27	N130927	32	1.8×10^6	1.4×10^4	—	—	0.01
NIF	Laser Indirect Drive	2013-11-19	N131119	32	1.9×10^6	1.7×10^4	—	—	0.01
NIF	Laser Indirect Drive	2017-06-01	N170601	1	1.5×10^6	4.8×10^4	—	—	0.03
NIF	Laser Indirect Drive	2017-08-27	N170827	1	1.7×10^6	5.3×10^4	—	—	0.03
NIF	Laser Indirect Drive	2019-09-18	N190918	30	1.9×10^6	2.1×10^4	—	—	0.01
NIF	Laser Indirect Drive	2019-10-07	N191007	1	1.9×10^6	5.3×10^4	—	—	0.03
NIF	Laser Indirect Drive	2019-11-10	N191110	30	1.9×10^6	5.6×10^4	—	—	0.03
OMEGA	Laser Direct Drive	2021	103952	13	3.0×10^4	8.7×10^2	—	—	0.03
OMEGA	Laser Direct Drive	2021	102360	13	3.0×10^4	7.5×10^2	—	—	0.02
OMEGA	Laser Direct Drive	2021	102154	13	3.0×10^4	6.3×10^2	—	—	0.02
NIF	Laser Indirect Drive	2021-02-07	N210207	1	1.9×10^6	1.7×10^5	—	—	0.09
NIF	Laser Indirect Drive	2021-03-07	N210307	5	1.9×10^6	1.4×10^5	—	—	0.07
NIF	Laser Indirect Drive	2021-08-08	N210808	5	1.9×10^6	1.3×10^6	—	—	0.69
JET	Tokamak	2021-12-21	99972	22	—	5.6×10^7	3.3×10^7	1.2×10^7	0.38
JET	Tokamak	2021-12-21	99971	22	—	5.9×10^7	3.1×10^7	1.0×10^7	0.33
OMEGA	Laser Direct Drive	2022	104949	16	3.0×10^4	5.9×10^2	—	—	0.02
NIF	Laser Indirect Drive	2022-09-19	N220919	5	2.0×10^6	1.2×10^6	—	—	0.59
NIF	Laser Indirect Drive	2022-12-04	N221204	5	2.0×10^6	3.1×10^6	—	—	1.51
NIF	Laser Indirect Drive	2023-07-30	N230730	11	2.0×10^6	3.9×10^6	—	—	1.89
JET	Tokamak	2023-10-03	104522	23	—	6.9×10^7	3.5×10^7	1.3×10^7	0.37
NIF	Laser Indirect Drive	2023-10-08	N231008	11	1.9×10^6	2.4×10^6	—	—	1.26
JET	Tokamak	2023-10-09	104600	23 and 24	—	2.7×10^7	3.5×10^7	4.0×10^6	0.11
NIF	Laser Indirect Drive	2023-10-30	N231030	11	2.2×10^6	3.4×10^6	—	—	1.55
NIF	Laser Indirect Drive	2024-02-12	N240212	11	2.2×10^6	5.2×10^6	—	—	2.36
NIF	Laser Indirect Drive	2024-11-18	N241118	33	2.2×10^6	4.1×10^6	—	—	1.86
NIF	Laser Indirect Drive	2025-02-23	N250223	33	2.0×10^6	5.0×10^6	—	—	2.44
NIF	Laser Indirect Drive	2025-04-07	N250406	12	2.1×10^6	8.6×10^6	—	—	4.13

- B. T. Klein, M. Mangan, T. Nagayama, A. J. Porwitzky, D. E. Ruiz, P. F. Schmit, S. A. Slutz, I. C. Smith, M. R. Weis, D. A. Yager-Elorriaga, D. J. Ampleford, K. Beckwith, T. R. Mattsson, K. J. Peterson, and D. B. Sinars, *Phys. Plasmas* **29**, 052711 (2022).
- ¹⁵S. McNamara, O. Asunta, J. Bland, P. Buxton, C. Colgan, A. Dnestrovskii, M. Gemmell, M. Gryaznevich, D. Hoffman, F. Janky, J. Lister, H. Lowe, R. Mirfayzi, G. Naylor, V. Nemytov, J. Njau, T. Pyragius, A. Rengle, M. Romanelli, C. Romero, M. Sertoli, V. Shevchenko, J. Sinha, A. Sladkomedova, S. Sridhar, Y. Takase, P. Thomas, J. Varje, B. Vincent, H. Willett, J. Wood, D. Zakhar, D. Battaglia, S. Kaye, L. Delgado-Aparicio, R. Maingi, D. Mueller, M. Podesta, E. Delabie, B. Lomanowski, and O. Marchuk, *Nucl. Fusion* **63**, 054002 (2023).
- ¹⁶V. Gopalaswamy, C. A. Williams, R. Betti, D. Patel, J. P. Knauer, A. Lees, D. Cao, E. M. Campbell, P. Farmakis, R. Ejaz, K. S. Anderson, R. Epstein, J. Carroll-Nellenbeck, I. V. Igumenshchev, J. A. Marozas, P. B. Radha, A. A. Solodov, C. A. Thomas, K. M. Woo, T. J. B. Collins, S. X. Hu, W. Scullin, D. Turnbull, V. N. Goncharov, K. Churnetski, C. J. Forrest, V. Y. Glebov, P. V. Heuer, H. McClow, R. C. Shah, C. Stoeckl, W. Theobald, D. H. Edgell, S. Ivancic, M. J. Rosenberg, S. P. Regan, D. Bredesen, C. Fella, M. Koch, R. T. Janezic, M. J. Bonino, D. R. Harding, K. A. Bauer, S. Sampat, L. J. Wexer, M. Labuzeta, S. F. B. Morse, M. Gutu-Johnson, R. D. Petrasco, J. A. Frenje, J. Murray, B. Serrato, D. Guzman, C. Shulberg, M. Farrell, and C. Deeney, *Nature Phys.* **20**, 751 (2024).
- ¹⁷C. Goyon, S. C. Bott-Suzuki, A. E. Youmans, J. T. Banasek, L. A. Morton, B. Levitt, J. R. Barhydt, K. D. Morgan, C. Liekhus-Schmaltz, W. C. Young, D. P. Higginson, A. C. Hossack, E. T. Meier, B. A. Nelson, M. Quinley, A. Taylor, P. Tsai, N. van Rossum, A. Shah, A. D. Stepanov, D. A. Sutherland, T. R. Weber, U. Shumlak, and H. S. McLean, *Phys. Plasmas* **31**, 072503 (2024).
- ¹⁸H. Gota, A. Smirnov, M. Binderbauer, T. Tajima, S. Putvinski, J. Titus, M. Nations, T. Roche, E. Trask, T. DeHaas, S. Detrick, E. Granstedt, D. Gupta, S. Gupta, A. Ivanov, S. Korepanov, R. Magee, T. Matsumoto, J. Romero, P. Yushmanov, K. Zhai, L. Schmitz, Z. Lin, S. Krasheninnikov, E. Baltz, J. Platt, E. Belova, T. Asai, A. Smolyakov, S. Abdollahi, S. Abramov, A. Alexander, I. Alfrey, R. Andow, D. Barnes, B. Barnett, J. Barrett, M. Beall, N. Bolte, E. Bomgardner, A. Bondarenko, F. Brightenti, J. Butterly, S. Caton, F. Ceccherini, Y. Choi, R. Clary, A. Cooper, C. Deng, A. de Vera, J. Drobny, A. Dunaevsky, C. Exton, A. Fareed, P. Feng, C. Finucane, D. Fluegge, A. Fontanilla, Y. Fujiwara, L. Galeotti, S. Galkin, R. Groenewald, T. Hsyu, K. Hubbard, R. Jaber, L. Jian, N. Kafle, S. Kamio, S. Karbashevski, J. Kinley, A. Korepanov, G. Koumarianou, S. Krause, P. Kudrin, C. Lau, H. Leinweber, J. Leuenberger, D. Lieurance, M. Litton, R. Luna, R. Luong, J. MacFarlane, D. Madura, J. Margo, D. Marshall, V. Matvienko, M. Meekins, W. Melian, R. Mendoza, R. Michel, M. Morehouse, Y. Mustafa, S. Nazarenko, A. Necas, B. Nick, N. Nwoke, S. Ohshima, M. Onofri, R. Page, J. Park, E. Parke, S. Patel, L. Penning, K. Phung, G. Player, L. Rios, I. Sato, J. Schroeder, Y. Shimabukuro, M. Showers, A. Sibley, M. Signorelli, M. Slepchenkov, R. Smith, G. Snitchler, V. Sokolov, D. Solyakov, Y. Song, B. Sporer, L. Steinhauer, C. Stonier, A. Stratta, J. Sweeney, M. Tobin, M. Tuszewski, J. Ufnal, T. Valentine, S. Vargas, A. Van Drie, V. Vekselman, A. Veksler, C. Weixel, C. White, M. Wollenberg, J. Wood, Y. Zhou, and S. Ziae, *Nucl. Fusion* **64**, 112014 (2024).
- ¹⁹H. Gota, (2024), private communication.
- ²⁰S. Howard, M. Reynolds, A. Froese, R. Zindler, M. Hildebrand, A. Mossman, M. Donaldson, T. Tyler, D. Froese, C. Eyrich, K. Epp, K. Bell, P. Carle, C. Gutjahr, A. Wong, W. Zawalski, B. Rablah, J. Sardari, L. McIlwraith, R. Bouchal, J. Wilkie, R. Ivanov, P. de Vietien, I. Khalzov, S. Barsky, D. Krotez, M. Delage, C. McNally, and M. Laberge, *Nucl. Fusion* **65**, 016029 (2024).
- ²¹A. Tancetti, C. Ribeiro, S. Howard, S. Coop, C. McNally, M. Reynolds, P. Kholodov, F. Braglia, R. Zindler, C. Macdonald, E. Love, P. Carle, X. Feng, A. Rohollahi, K. Leci, D. Plant, C. Dunlea, R. Ivanov, and A. Mossman, *Nuclear Fusion* **65**, 036043 (2025).
- ²²M. Maslov, E. Lerche, F. Auriemma, E. Belli, C. Bourdelle, C. Challis, A. Chomiczewska, A. Dal Molin, J. Eriksson, J. Garcia, J. Hobirk, I. Ivanova-Stanik, P. Jacquet, A. Kappatou, Y. Kazakov, D. Keeling, D. King, V. Kiptily, K. Kirov, D. Kos, R. Lorenzini, E. De La Luna, C. Maggi, J. Mailloux, P. Mantica, M. Marin, G. Matthews, I. Monakhov, M. Nocente, G. Pucella, D. Rigamonti, F. Rimini, S. Saarelma, M. Salewski, E. Solano, Z. Štancar, G. Stankunas, H. Sun, M. Tardocchi, and D. Van Eester, *Nuclear Fusion* **63**, 112002 (2023).
- ²³A. Kappatou, M. Baruzzo, A. Hakola, E. Joffrin, D. Keeling, B. Labit, E. Tsitrone, N. Vianello, M. Wischmeier, I. Balboa, J. Bernardo, M. Bernert, T. Bosman, S. Brezinsek, D. Brida, I. S. Carvalho, P. Carvalho, L. Ceelen, C. D. Challis, I. Coffey, T. Dittmar, M. Dunne, M. Faitsch, A. R. Field, L. Frassinetti, L. Garzotti, Z. Ghani, C. Giroud, S. Henderson, R. B. Henriques, J. Hobirk, P. Jacquet, I. Jepu, Y. O. Kazakov, D. B. King, K. K. Kirov, D. Kos, K. Krieger, M. Lennholm, E. Lerche, X. Litaudon, E. Litherland-Smith, P. Lomas, C. Lowry, J. Mailloux, M. J. Mansinen, M. Maslov, D. Matveev, A. Meigs, S. Menmuir, C. Olde, C. Perez von Thun, L. Piron, G. Pucella, H. Reimerdes, F. Rimini, O. Sauter, P. A. Schneider, B. Sieglin, S. Silburn, E. R. Solano, H. Sun, D. F. Valcarcel, D. van Eester, R. Villari, A. Widdowson, S. Wiesen, M. Zlobinski, V. K. Zotta, t. J. contributors, and t. E. Tokamak Exploitation Team, *Plasma Physics and Controlled Fusion* **67**, 045039 (2025).
- ²⁴I. Carvalho, C. Giroud, D. King, D. Keeling, L. Frassinetti, R. Pitts, S. Wiesen, G. Pucella, A. Kappatou, N. Vianello, M. Wischmeier, F. Rimini, M. Baruzzo, M. Maslov, M. Sos, X. Litaudon, R. Henriques, K. Kirov, C. Thun, H. Sun, M. Lennholm, J. Mitchell, A. Parrot, J. Bernardo, M. Zerbini, I. Coffey, K. Collie, J. Fontdecaba, N. Hawkes, Z. Huang, I. Jepu, D. Kos, K. Lawson, E. Litherland-Smith, A. Meigs, C. Olde, A. Patel, L. Piron, M. Poradzinski, Z. Stancar, D. Taylor, E. Alessi, I. Balboa, A. Boboc, S. Bakes, M. Brix, E. De la Cal, P. Carvalho, A. Chomiczewska, et al., J. Karhunen, JET Contributors, and EUROfusion Tokamak Exploitation Team, “Neon seeded iter baseline scenario experiments in jet d and d-t plasmas,” in *50th EPS Conference on Plasma Physics, EPS 2024*, European Physics Conference Abstracts, edited by J. Kirk and L. Volpe (European Physical Society, France, 2024) ext abstract; 50th EPS Conference on Plasma Physics, EPS 2024 ; Conference date: 08-07-2024 Through 12-07-2024.
- ²⁵M. J. Singh, D. Boilson, A. R. Polevoi, T. Oikawa, and R. Mitteau, *New J. Phys.* **19**, 055004 (2017).
- ²⁶O. Meneghini, P. B. Snyder, S. P. Smith, J. Candy, G. M. Staebler, E. A. Belli, L. L. Lao, J. M. Park, D. L. Green, W. Elwasif, B. A. Grierson, and C. Holland, *Phys. Plasmas* **23**, 042507 (2016).
- ²⁷F. Wagner, S.-I. Itoh, S. Inagaki, M. Shindo, and M. Yagi, *AIP Conf. Proc.* **1095**, 31 (2009).
- ²⁸O. Meneghini, G. Snoep, B. Lyons, J. McClenaghan, C. Imai, B. Grierson, S. Smith, G. Staebler, P. Snyder, J. Candy, E. Belli, L. Lao, J. Park, J. Citrin, T. Cordemiglia, A. Tema, and S. Mordijk, *Nucl. Fusion* **61**, 026006 (2020).
- ²⁹V. Mukhovatov, Y. Shimomura, A. Polevoi, M. Shimada, M. Sugihara, G. Bateman, J. Cordey, O. Kardaun, G. Pereverzov, I. Voitsekhovich, J. Weiland, O. Zolotukhin, A. Chudnovskiy, A. Kritz, A. Kulushkin, T. Onjun, A. Pankin, and F. Perkins, *Nucl. Fusion* **43**, 942 (2003).
- ³⁰A. B. Zylstra, A. L. Kritcher, O. A. Hurricane, D. A. Callahan, K. Baker, T. Braun, D. T. Casey, D. Clark, K. Clark, T. Döppner, L. Divol, D. E. Hinkel, M. Hohenberger, C. Kong, O. L. Landen, A. Nikroo, A. Pak, P. Patel, J. E. Ralph, N. Rice, R. Tommasini, M. Schoff, M. Stadermann, D. Strozzi, C. Weber, C. Young, C. Wild, R. P. J. Town, and M. J. Edwards, *Phys. Rev. Lett.* **126**, 025001 (2021).
- ³¹M. Keilhacker, A. Gibson, C. Gormezano, P. Lomas, P. Thomas, M. Watkins, P. Andrew, B. Balet, D. Borba, C. Challis, I. Coffey, G. Cottrell, H. D. Esch, N. Deliyanakis, A. Fasoli, C. Gowers, H. Guo, G. Huysmans, T. Jones, W. Kerner, R. König, M. Loughlin, A. Maas, F. Marcus, M. Nave, F. Rimini, G. Sadler, S. Sharapov, G. Sips, P. Smeulders, F. Söldner, A. Taroni, B. Tubbing, M. v. Hellermann, D. Ward, and J. Team, *Nuclear Fusion* **39**, 209 (1999).
- ³²O. A. Hurricane, D. A. Callahan, D. T. Casey, P. M. Celliers, C. Cerjan, E. L. Dewald, T. R. Dittrich, T. Döppner, D. E. Hinkel, L. F. B. Hopkins, J. L. Kline, S. Le Pape, T. Ma, A. G. MacPhee, J. L. Milovich, A. Pak, H.-S. Park, P. K. Patel, B. A. Remington, J. D. Salmonson, P. T. Springer, and R. Tommasini, *Nature* **506**, 343 (2014).
- ³³LLNL, LLNL NIF & Plasma Science Website (2025), available at <https://lasers.llnl.gov/science/achieving-fusion-ignition>.

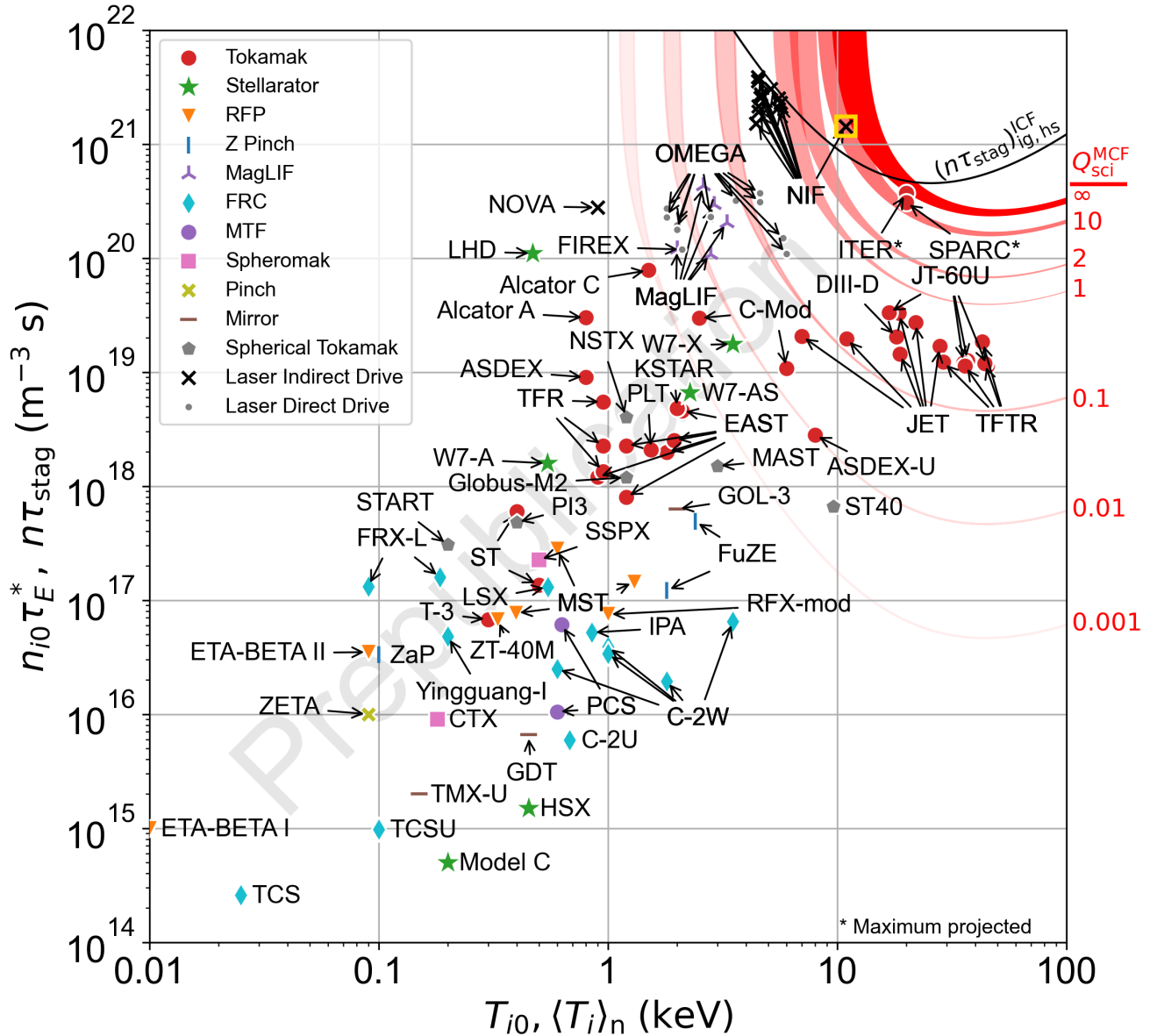


FIG. 1. Experimentally inferred Lawson parameters ($n_{i0} \tau_E^*$ for MCF and $n \tau_{\text{stag}}$ for ICF) of fusion experiments vs. T_{i0} for MCF and $\langle T_i \rangle_n$ for ICF (see Sec. III of the original paper for definitions of these quantities), extracted from the published literature (see Tables I–III). The red contours correspond to the Lawson parameters and ion temperatures required to achieve the indicated values of scientific gain for an advanced-tokamak (AT) model, which may be considered generally representative of MCF and are labeled as $Q_{\text{sci}}^{\text{MCF}}$. The contour colors in the original paper have been replaced by varying shades of red here to emphasize that they originate from a tokamak model. The finite widths of the $Q_{\text{sci}}^{\text{MCF}}$ contours represent a range of assumed impurity levels. The black curve corresponds to the Lawson parameters and ion temperatures required to achieve hot-spot ignition and the onset of propagating burn for direct- and indirect-drive laser ICF and is labeled $(n \tau_{\text{stag}})_{\text{ig,hs}}^{\text{ICF}}$. See caption of Fig. 3 regarding the gold box on one of the NIF data points. For all contours, we assume representative density and temperature profiles, external-heating absorption efficiencies, and D-T fuel. For experiments that do not use D-T, the contours represent a D-T-equivalent value. See Sec. IV of the original paper and Sec. III C of this paper for details on how the $Q_{\text{sci}}^{\text{MCF}}$ and $(n \tau_{\text{stag}})_{\text{ig,hs}}^{\text{ICF}}$ contours are calculated and how individual data points are extracted.

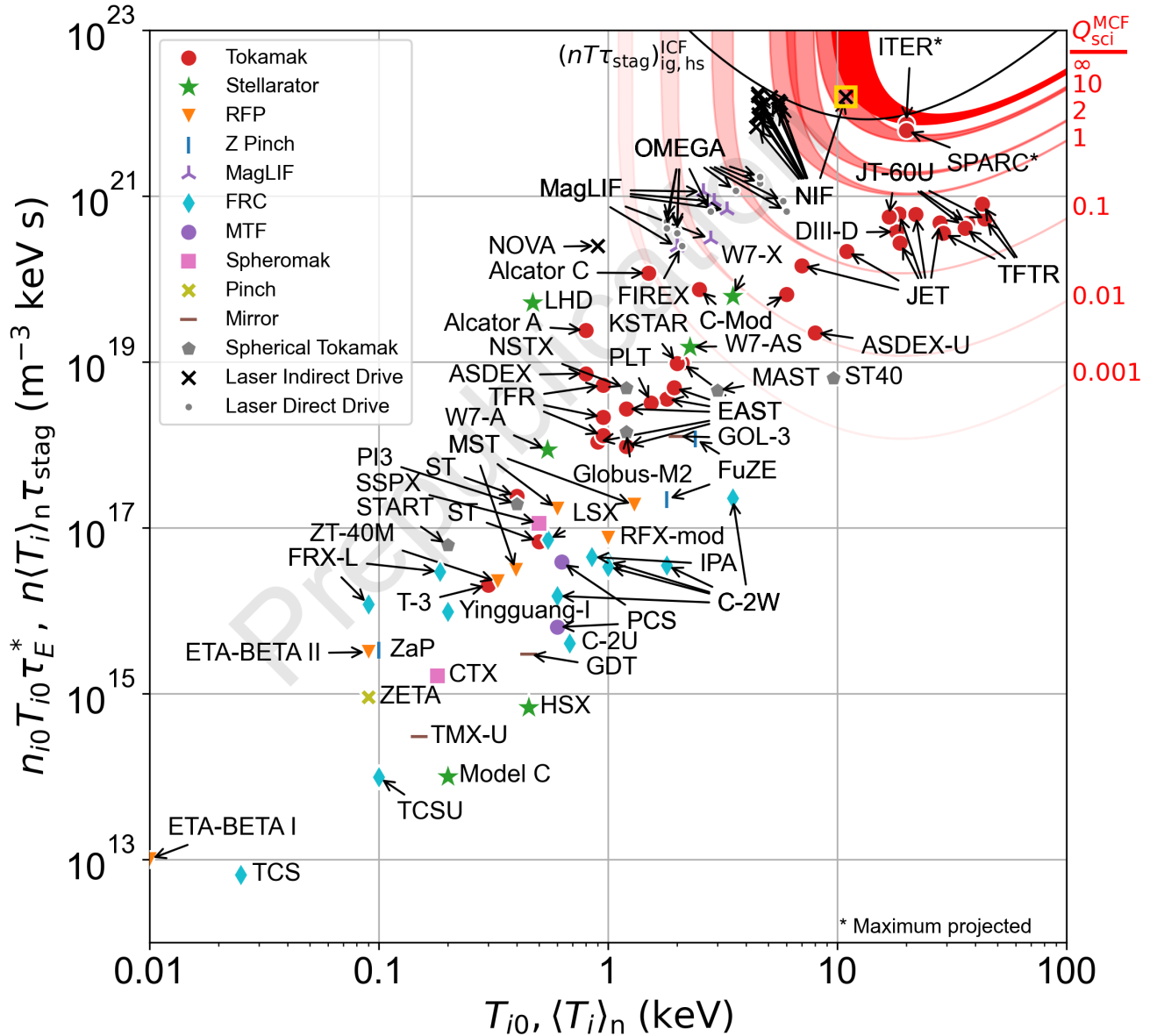


FIG. 2. Experimentally inferred triple products of fusion experiments vs. ion temperature, extracted from published literature. See the caption of Fig. 1 for more details, and the caption of Fig. 3 regarding the gold box around one of the NIF data points.

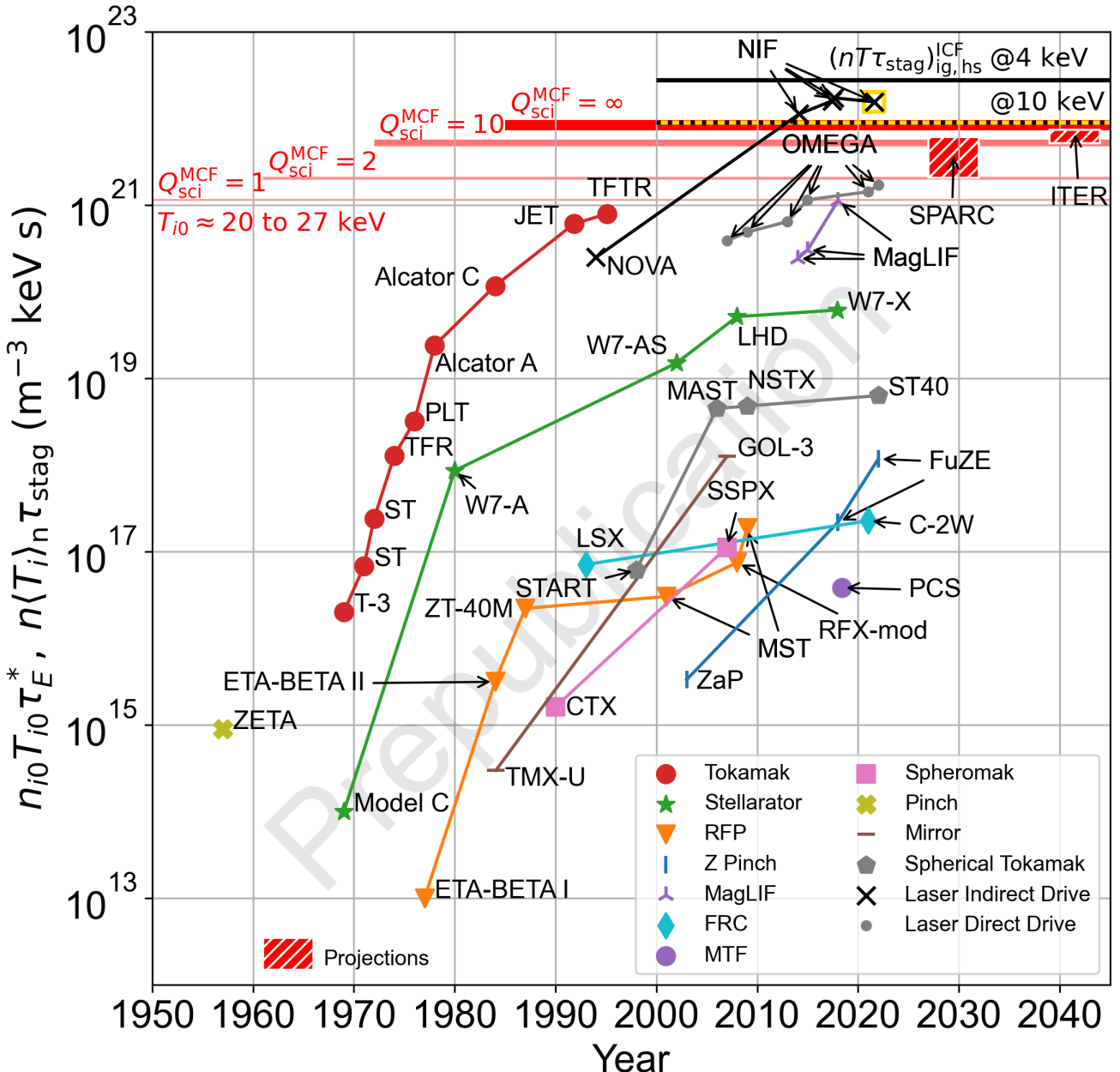


FIG. 3. Triple products $(n_{i0} T_{i0} \tau_E^*, n \langle T_i \rangle_n \tau_{\text{stag}})$ for MCF and $n \langle T_i \rangle_n \tau_{\text{stag}}$ for ICF, as defined in Sec. III of the original paper and updated in Sec. III C of this paper) that set a record for a given concept vs. year achieved. Record values for different concepts are shown to illustrate the progress towards energy gain of different concepts over time. The horizontal lines labeled $Q_{\text{sci}}^{\text{MCF}}$ represent the minimum required triple product to achieve the indicated values of $Q_{\text{sci}}^{\text{MCF}}$. The thickness of these lines are equal to the thickness of the equivalent contours in Fig. 2 at their minimum values. The central ion temperatures required to achieve the minimum triple products (corresponding to the indicated values of scientific gain on Fig. 16 of the original paper) are in the range 20 keV to 27 keV, which is now indicated on the plot. The black horizontal line labeled “ $(n T \tau_{\text{stag}})^{\text{ICF}} @ T_i = 4 \text{ keV}$ ” represents the required triple product to achieve ignition and the onset of propagating burn in an ICF hot spot, assuming $T_i = 4 \text{ keV}$. The dashed gold-and-black horizontal line labeled “ $@ T_i = 10 \text{ keV}$ ” represents the required triple product to achieve ignition and the onset of propagating burn in an ICF hot spot, assuming $T_i = 10 \text{ keV}$. Although the NIF shot from August 8, 2021 did not set a triple-product record, we include it in this updated plot because it achieved hot-spot ignition and the onset of propagating burn and is an appropriate terminal data point for NIF on this plot and have added a gold box to highlight this fact. This final data point for NIF lies below the black line (and was not a record triple product because stagnation time τ_{stag} for an ignited fuel assembly is depressed due to the more rapid disassembly that results from the dynamics of an ignited hot spot), but it did achieve $T_i > 10 \text{ keV}$ and is above the dashed gold-and-black horizontal line, which denotes the hot-spot ignition and onset of propagating burn requirement at 10 keV. See Sec. III D of this paper and Sec. IV B 4 of the original paper for a discussion of the limitations of using the triple product as a figure of merit for experimental results near and beyond ignition for ICF. More recent and even higher-performing NIF shots (including exceeding scientific breakeven for N221204) are not shown on this plot but are shown on Fig. 4. The projected triple-product ranges for SPARC and ITER are bounded above by their projected peak triple products and below by the original stated missions of each experiment (i.e., $Q_{\text{fuel}}^{\text{MCF}} = 2$ for SPARC and $Q_{\text{fuel}}^{\text{MCF}} = 10$ for ITER). The timelines for both SPARC and ITER have been delayed since the publication of the original paper, and the most recently announced timelines³⁴ are reflected here.

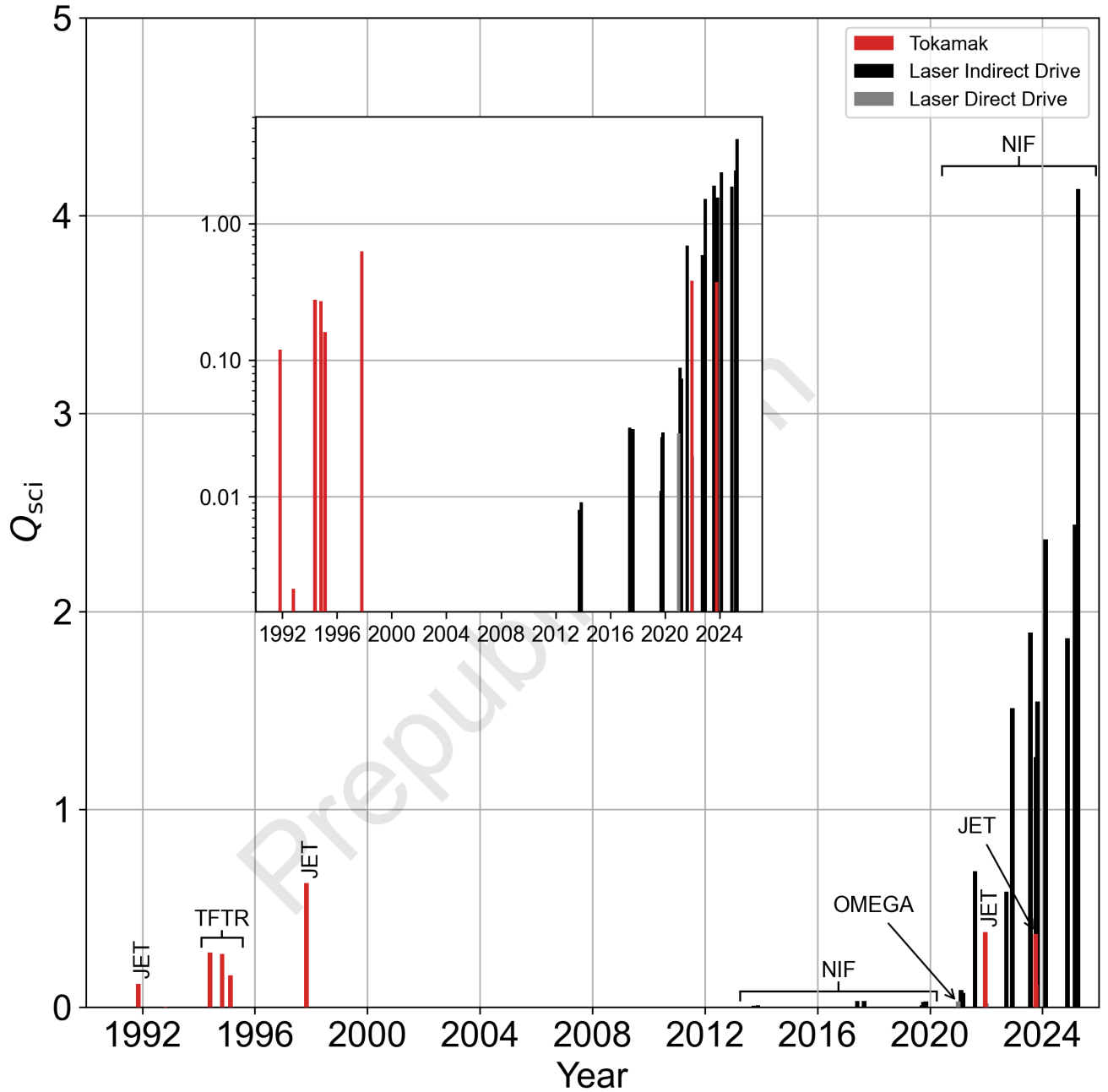


FIG. 4. Plot of actual Q_{sci} vs. date achieved for D-T fusion experiments. Inset plot shows the same data on log-linear axes. Values of Q_{sci} for NIF and OMEGA results are reported on an energy basis ($Q_{\text{sci}} = Y/E_{\text{in}}$, where Y is the fusion energy yield and E_{in} is the laser energy). Values of Q_{sci} for JET and TFTR are reported on a power basis ($Q_{\text{sci}} = P_{\text{F}}/P_{\text{in}}$, where P_{F} is fusion power and P_{in} is heating power crossing the vacuum-vessel boundary). JET shots 99971 and 99972 (taken on the same day in 2021) use power levels averaged over 5 and 2 s, respectively. JET shots 104522 and 104600 (taken in 2023) use power levels averaged over 3 and 5 s, respectively. Earlier shots from JET and TFTR (from the 1990s) are instantaneous values taken at the time of peak fusion energy production.